PCCP

Accepted Manuscript

ROYAL SOCIETY OF CHEMISTRY

www.rsc.org/pccp

Adatom Transport through (√3 × √3)–R30°–CH_3S self-assembled monolayers on Au(111) from first principles

D. Paulius[a], D. Torres[b] F. Illas[c] and W. E. Archibald[a]

[a]*College of Science and Mathematics, University of the Virgin Islands, The Virgin Islands*

[b]*Department of Science, BMCC-CUNY, New York, NY 10007 (USA)*

[c]*Departament de Química Física & Institut de Química Teòrica i Computacional (IQTCUB), Universitat de Barcelona, 08028 Barcelona, Spain*

Abstract

Self-assembled monolayers on Au(111) have outstanding chemical, electrical, and optical properties, and Au adatoms seem to play a key role on these properties. Still, the fundamental understanding of adatom transport inside the self-assembly is very sparse. In this paper we use first-principles calculations to reveal new details about the migration mechanism of Au adatoms in the presence of CH_3S self-assembly on Au(111). We study the inclusion of Au adatoms inside a well-packed (√3×√3)–R30°–CH_3S self-assembled lattice and present atomistic models supporting adatom migration by means of a hopping mechanism between pairs of CH_3S species. Our calculations reveal that the transport of Au adatoms is slowed down inside the molecular network where the kinetic barrier for adatom migration is larger than on the clean Au surface. We attribute the hindered mobility of Au adatoms to the fact that adatom transport involves the breaking and making of Au-S bonds. Our results form a basis for further understanding the role played by defect transport in the properties of molecular assemblies.

Introduction

The design and fabrication of metallic surfaces with well-defined structure at the nanometer scale is a challenge hardly achievable by large-scale top-down procedures. Not surprisingly, the self-assembly process has become a potent bottom-up approach which allows one to vanquish these difficulties.[1,2] Self-assembled monolayers (SAMs) on metallic surfaces, in particular on Au surfaces, offer a spectrum of promising applications such as chemical sensors, lubricating layers or corrosion inhibitors.[3-5] Well-organized alkanethiol SAMs coatings can modify, for example, the catalytic properties of the metallic substrate[6] and their attractive electrical and optical properties have been used to improve the efficiency of dye-sensitized solar cells based devices.[7] Despite the fact that much effort has been invested in the study of the morphology of self-assembled structures, as shown in recent reviews,[8-10] to understand the role of defect in SAMs still remains a challenge.

Extensive studies consistently demonstrated that self-assembly generates surface defects such as vacancies and surface adatoms, and it is generally accepted that defects play an important role on the overall self-assembly process.[11-14] STM studies identified the extraction of surface Au atoms during self-assembly and the presence of Au vacancies at the interface was suggested by Density Functional Theory (DFT) based calculations.[15] These adatoms incorporate into the self-assembly at low coverage forming stripped phases as in the case of the so-called MT-Au-MT complex with a central Au adatom linearly coordinated to two methylthiolates (MT).[16] Studies by Maksymovych et al.[17] corroborate this finding whereas the pioneering studies by Weiss et al.[16] demonstrated that Au adatoms migrate through the surface by means of the transport of the whole MT-Au-MT complex. In previous studies it has been shown that, in spite of significant differences in atomic structure, different surface models with different atomic structure can have similar thermodynamic stability, and we further proved that the self-assembly process reduces the energy required to strip an atom from the Au surface, the thermodynamic driving force for atom stripping being more favourable along step-edge lines within the self-assembled structure.[18,19] The necessity to understand the role played by surface defects on self-assembly has inspired years of surface science research. Still, detailed information on adatom transport, in particular in the high-coverage regime, is scarce, and the relevance of these predictions is rarely discussed in the literature.

In this work we address the properties and diffusion mechanism of Au adatoms inside a well-packed ($\sqrt{3}\times\sqrt{3}$)–R30°–CH_3S self-assembled lattice on Au(111) and present atomistic

models supporting the transport of Au adatoms through a hopping mechanism between pairs of methylthiolates. Our calculations reveal that the mobility of Au adatoms inside the self-assembled network is reduced compared to the situation on a clean Au surface and that the migration of Au adatoms inside the assembly is hindered by a larger energy barrier. In contrast, Au adatoms in a clean Au surface or at early stages of self-assembly transport with a smaller energy barrier. These observations are consistent with the fact that the CH_3S-mediated transport of adatoms by means of a hopping mechanism involves the breaking and making of Au-S bonds, which increases the effective energy barrier for adatoms migration. The present results thus form a basis for further understanding the role played by defect transport in the properties of molecular assemblies.

Surface models and computational details

The diffusion mechanism of Au adatoms in the presence of a self-assembly adsorbed on Au(111) has been studied using DFT based periodic calculations carried out as implemented in the Vienna Ab Initio Simulation Package (VASP).[20,21] The DFT calculations employ the projector-augmented wave method [22] to describe the effect of the atomic cores in the valence density in conjunction with a plane-wave basis set (cutoff energy of 400 eV) to expand the valence density and the PW91 implementation[23] of the generalized gradient approach (GGA) to the electronic exchange and correlation potential which predicts binding energies and geometries in qualitative agreement with experiment. Recently, it has been shown that this type of GGA functional provides a well-balanced description of the three series of transition metals in the periodic table.[24] Van der Waals dispersion forces were not considered in this study because they are known to have little effect for small adsorbates on metallic surfaces as recently shown for the case of CH4 on several Ni flat and stepped surfaces.[25] A stronger influence appears on larger adsorbates with multiple contacts with the metallic surface[26] thus affecting the organization and stability of longer alkanethiol monlayers.[27]

The Au(111) surface is represented by a slab model consisting of five metallic layers with a total of 135 Au atoms in the unit cell interleaved by a vacuum space of ~10 Å. The two outermost atomic metal layers as well as the atomic coordinates of MT moieties were allowed to relax without further constraints. To model the MT adsorption on the Au(111) surface we employed a $(3\sqrt{3} \times 3\sqrt{3})$-R30°-9$CH_3S$ unit cell which has been previously observed for this adsorbate in the high coverage regime. In this structure, the nine CH_3S moieties included in the unit cell are located at *bridge* sites as shown in Figure 1 (Top panel). The calculated

average adsorption height of the CH_3S species above the Au(111) surface plane was 2.01 Å and the average tilt angle between the surface normal and the S-C bond was 52°, in concordance with previous studies.[28] Note that there is also an experimental report suggestion that this phase can be transformed into a (3 × 2√3) structure by thermal annealing.[29] This lattice, however, has rarely been observed for MT on Au(111) although (3× 2√3) and c(4× 2) structures are often found for longer alkanethiol chains.[30] The interaction of a single Au adatom with the clean surface (3√3 × 3√3) unit cell gives a low-enough 0.037 Au gold coverage. Because of the large unit cell size, the Brillouin zone integration was carried out at the Γ point only. This is the usual approach for ***k***-point interaction in the reciprocal for large enough supercells. In fact, test calculations carried out using a denser grid of special ***k***-points indicate that calculations involving the Γ point only are converged up to 0.01 eV. We employed the same Au unit cell to model the SCH_3-Au-SCH_3 complex adsorption.

Formation energies of self-assembled phases, E^f, were computed with respect to bulk Au and gas phase dimethyl-thiolate (DMT) as in Eq. 1

$$E^f = E_{Au\text{-}SAM} - E_{Au}^{Bulk} - N_{MT}E_{DMT}/2 - E^{Au}_{cell}, \quad (1)$$

where $E_{Au\text{-}SAM}$ is the energy of self-assembled phase within the (3√3 × 3√3)-R30°-9CH_3S unit cell containing one Au adatom and E_{Au}^{Bulk}, E^{Au}_{cell} and E_{DMT} are the energy of a bulk Au atom, the energy of the clean Au(111) slab (3√3 × 3√3) unit cell and the total energy of gas phase DMT, respectively. We referred the formation energies to DMT and hence, E_{DMT} was divided by two in order to account the right number of CH_3S species. N_{MT} stands for the number of MT species in the unit cell (two for the CH_3-Au-CH_3 complexes and nine for the packed SAMs phases).

Transition-state (TS) structures were located through the climbing image-nudged elastic band method (CI-NEB),[31-33] using 33 interpolated images along the minimal-energy pathway, which allowed the description of an almost continuous energy path. All minima on the potential energy surface were relaxed until self-consistent forces are lower than 0.01 eV/Å and TS structures were fully characterized with a pertinent vibrational analysis through diagonalization of the Hessian matrix obtained by numerical difference of analytical gradients and making sure TS structures show a single normal mode associated with an imaginary frequency connecting the two energy minima.

Results and discussion

In order to gain insight into the adsorption energetics of Au adatoms inside the packed

self-assembly, we will first screen the potential energy surface of the SCH_3 network. The binding energies for the most representatives adsorption sites inside the self-assembly, together with characteristic structural parameters–labelled depending on the location of the adatom–are listed in Tables 1 and 2, whereas the adsorption structures are depicted in Figure 1. Our calculations reveal that SCH_3 species mediate the adsorption of Au adatoms, and the most stable adsorption arrangement corresponds to the *fcc* configuration where the Au adatom located on a *fcc* site is bonded to two different SCH_3 species along the <01$\underline{1}$> direction on *top-fcc* sites respectively. The adsorbed adatom is located 2.53 Å above the (111) surface plane, this distance being only 0.2 Å larger than the corresponding value for an isolated Au adatom. The average Au-S bond distance is ~2.3 Å and the S-C bonds are tilted away from the surface normal an average angle of 66°. The majority of the adsorption sites for Au adatom inside the self-assembly are energetically very similar, with binding energies E^f between −2.2 and −2.4 eV, which are indicative of a very flat PES for adatom adsorption. Our calculations further reveal that adsorption arrangements involving only a single Au-SCH_3 bond are energetically less stable compared to the SCH_3-Au-SCH_3 arrangement. As an example of this, E^f for the *top'* site depicted in Figure 1 is −1 eV, a considerably more endothermic value than the average double-coordinated adatom.

The model calculations discussed above reveal that the geometry of Au adatoms adsorbed inside the self-assembly closely resembles the structure of a SCH_3-Au-SCH_3 complex. Note that this type of complex is thought to be actively involved in the SAM nucleation mechanism. In order to achieve deeper insight into the structural similarities of both moieties we have optimized a set of SCH_3-Au-SCH_3 complexes on the Au(111) surface resembling the geometry of some of the self-assembled phases described above. The adsorption configurations are depicted in Figure 2 and geometric parameters are collected in Table 3. The different possible rotational isomers — resulting mainly from rotations involving the CH_3-group around the S-C bond — and stereoisomers — resulting for different SCH_3 orientations — both are known to produce minor energy changes and were not considered in this study.[34] Our computed geometries, in good agreement with previous DFT results[34], show that the Au adatom at the *fcc* SCH_3-Au-SCH_3 complex is adsorbed 2.50 Å above the Au(111) surface plane, whereas the SCH_3 radicals are bonded to the central Au adatom with average Au-S distance of ~2.3 Å, the S-C bonds being tilted toward the Au surface by an average angle of 65°. An estimate for the smallest diffusion barrier for the Au adatom attached to the CH_3S-Au-CH_3S complex was found to be ΔE=0.20 eV, corresponding to the energy difference between the most stable *bridge* arrangement and a *top* sites, this value

being consistent with previous studies.

The electronic structure of the Au adatom at a SCH_3-Au-SCH_3 complex and inside the SAM phase are also very similar. In Figure 3 we display projected Density of State (PDOS) plots for the most stable *fcc* site on the self-assembly and for the most stable CH_3S-Au-CH_3S complex with the Fermi level set as the origin of the energy scale. Our results demonstrate that the states of the Au adatom are similarly hybridized with the CH_3S states, suggesting that the CH_3S–Au bonds on the self-assembled phase have similar strength than on a CH_3S-Au-CH_3S moiety.

We now focus into the transport/diffusion of Au adatoms within the well-packed SAM along the <$\underline{1}$01> and <1$\underline{1}$0> high symmetry directions of the corresponding lattice. These two symmetry directions follow the periodicity of the SAM lattice. Further diffusion directions can be considered by combining the results of the <$\underline{1}$01> and <1$\underline{1}$0> symmetry directions. Atomistic ball model illustrating the assembly-mediated diffusion pathways along the <$\underline{1}$01> and <1$\underline{1}$0> directions are displayed in Figure 4, whereas Tables 4 and 5 collect the geometries and binding energies for the transition states involved in the mechanism.

The simplest imaginable self-assembly-mediated diffusion mechanism would involve adatom hopping between different CH_3S pairs forming consecutive CH_3S-Au-CH_3S complexes. Indeed, the spontaneous diffusion of Au adatoms *via* adatoms hop between pairs of methylthiolate species inside the well-packed SAM was recently observed.[35] Subsequent to this initial step (step 1) where the Au adatom migrates from the most stable *fcc* site to a *top* site, the Au adatom will then diffuse into an *hcp* hollow site (step 2), to finally return to and equivalent *fcc* site by means of a path involvong *bridge* site (step 3). This CH_3S-mechanism would eventually lead to adatom diffusion along the <$\underline{1}$01> direction. Steps 1 and 2 limit the migration along the <$\underline{1}$01> direction, the kinetic barriers for the migration being 0.9 and 0.7 eV, respectively. The migration step involves the breaking of an existing Au-S bond along the <01$\underline{1}$> with the concomitant creation of a new Au-S bond with a new CH_3S species along the <1$\underline{1}$0> direction. As an example of this, for migration through step 2, the Au-S distances vary from 2.69 Å at the staring *Top* site to 3.45 Å at the final *hcp* site, with intermediate values of 2.75 Å at the transition state, as shown in Figure 5 (Top Central Panel). The *hcp*-to-*fcc* transition (step 3) proceeds by means of a small ~0.1 eV activation barrier and involves minimum rearrangement on the self-assembly.

The diffusion process along the <1$\underline{1}$0> direction starts by means of a *fcc*-to-*hcp'* transition (step 1') followed by *a hcp'*-to-*fcc'* transition (step 2'). The kinetic barrier for the

first step is 1.1 eV and the migration step involves the breaking and creation of an Au-S bond, with a bridge-like transition state characterized by a 2.77 Å Au-S distance. The following *hcp'*-to-*fcc'* transition, with a small 0.1 eV barrier, involves minor geometrical changes. Finally, from the *fcc'* site, the Au adatom would jump into a *hcp* site (step 3') which eventually will lead back to a symmetrically equivalent *fcc* site. The fcc'-to-hcp transition limit the diffusion along the <1$\underline{1}$0> direction with a kinetic barrier of ~1 eV, and on this transition, the Au-S bond elongates from 2.34 Å to 3.45 Å with an intermediate value of 2.81 Å at the transition state.

The mechanism described above contrasts with that involving Au adatoms in a clean Au surface or at early stages of self-assembly where CH_3S-Au-CH_3S complexes can easily transport with a rather low energy cost. In fact, the transport of Au adatoms by means of a hopping mechanism between pairs of methylthiolates involves the breaking and creation of Au-S bonds. This increases the effective energy barrier for adatom migration, which indicates that inside the well-packed self-assembled network the mobility of gold adatoms is hindered. Temperature effects are also expected to play a key role, reducing the effective diffusion rate although not affecting the energy barriers derived from the potential energy surface which, obviously correspond to 0K. Temperature can, however, have a small effect on the free energy potential energy surface mainly through the vibrational contribution. However, this would not affect the main conclusion arising from the present results, namely that high temperatures would be needed to activate Au adatoms trapped inside the self-assembly. In fact, the present results agree with the experimental observations suggesting that MT adsorbates reduce the rate of motion of the attached gold.[4] Therefore, Au adatoms would help transport MT molecules by slowing down the mass transport when the molecular assembly is fully formed. Our results form a basis for further understanding the role played by defect transport in the properties of molecular assemblies.

Conclusions

To summarize, we presented atomistic models characterizing adatom migration inside the well-packed ($\sqrt{3} \times \sqrt{3}$)-R30°-CH_3S self-assembled lattice by means of first-principles simulations. Our results, obtained from density functional calculations on a large enough ($3\sqrt{3} \times 3\sqrt{3}$)-R30°-$CH_3S$ supercell containing 9 independent MT molecules and a single Au adatom revealed that the mobility of gold adatoms inside the well-packed self-assembled network is reduced, compared to the early stages of self-assembly grow or even to clean gold. We presented atomistic models characterizing the transition states underlying adatoms

migration in order to support the reduced mass transport of gold adatoms. Thus, the present results form a basis for further understanding the role played by defect transport in the properties of molecular assemblies.

Acknowledgments.

The calculations utilized resources at the BNL Center for Functional Nanomaterials (CFN) and the New York Center for Computational Sciences (NYCCS). Additional support from Spanish MINECO CTQ2012-30751 research grant and partial support from Generalitat de Catalunya 2014SGR97 and XRQTC grants is accredited. F.I. acknowledges support from the 2009 ICREA Academia award for excellence in research. W.E.A. wishes to acknowledge startup funding from the University of the Virgin Islands support of energy development grant.

Table 1. Structural and energetic parameters characterizing the adsorption of a single Au adatom in the (3√3 × 3√3)-R30°-9CH_3S self-assembly involving a S-Au-S bond along the <1$\underline{1}$0> and <0$\underline{1}$1> directions. Structures are displayed in Figure 2. E^f – Formation energy for the SAM phase refered to the clean Au(111) suface, gas phase $(CH_3S)_2$ and bulk Au; $z_e(Au)$ – Equilibrium height of Au over the surface (111) plane; $z_e(S)$ – Average equilibrium height of the two S atoms bonded to the Au adatom over the surface (111) plane; d_e(Au-S) – Average interatomic distance between the Au adatom and two of the nearest S atoms; d_e(S-C) – Average interatomic S-C distance for the two CH_3 species bonded to Au in the self-assembly.

Parameter	*top*	*bridge*	*fcc*	*hcp*
E^f, eV	-2.25	-2.19	-2.37	-2.31
z_e(Au), Å	2.619	2.447	2.532	2.455
z_e(S), Å	2.689; 2.220	2.600; 2.821	2.642; 2.210	2.685; 2.127
d_e(Au-S), Å	2.320	2.350	2.346	2.350
d_e(S-C), Å	1.830	1.834	1.834	1.826

Table 2. Structural and energetic parameters characterizing the adsorption of a single Au adatom in the the $(3\sqrt{3} \times 3\sqrt{3})$-R30°-9$CH_3S$ self-assembly involving a S-Au-S bond along the <101> direction. Structures are displayed in Figure 2. E^f – Formation energy for the SAM phase refered to the clean Au(111) suface, gas phase $(CH_3S)_2$ and bulk Au; $z_e(Au)$ – Equilibrium height of Au over the surface (111) plane; $z_e(S)$ – Average equilibrium height of the two S atoms bonded to the Au adatom over the surface (111) plane; d_e(Au-S) – Average interatomic distance between the Au adatom and two of the nearest S atoms; d_e(S-C) – Average interatomic S-C distance for the two CH_3 species bonded to Au in the self-assembly.

Parameter	*top'*	*bridge'*	*fcc'*	*hcp'*
E^f, eV	-1.01	-2.25	-2.19	-2.29
z_e(Au), Å	2.514	2.593	2.564	2.461
z_e(S), Å	2.599; 2.221	2.570; 2.574	3.217; 2.656	2.647; 2.461
d_e(Au-S), Å	2.334	2.350	2.354	2.345
d_e(S-C), Å	1.820	1.825	1.834	1.826

Table 3. Calculated parameters characterizing the MT-Au-MT adsorption on the most stable sites of the Au(111) metal surface. Structures are displayed in Figure 1. E^f – Formation energy of the complex refered to the clean Au(111) suface, gas phase $(CH_3S)_2$ species and bulk Au; z_e(Au), z_e(S) – Equilibrium height of Au and the two S atoms, respectively, over the surface (111) plane; d_e(Au-S), d_e(S-C) – Average interatomic average Au-S and S-C distances; □□$_e$(S-Au-S) – S-Au-S dihedral angles formed between the two C-S-Au planes of the CH_3S-Au-CH_3S complex and the surface normal.

Parameter	*top*	*bridge*	*fcc*	*hcp*
E^f, eV	-1.15	-1.35	-0.75	-1.07
z_e(Au), Å	2.675	2.50	2.497	2.548
z_e(S), Å	2.685; 2.821	2.653; 2.556	3.074; 2.601	2.838; 2.675
d_e(Au-S), Å	2.331	2.335	2.354	2.329
d_e(S-C), Å	1.830	1.833	1.838	1.838
□$_e$(S-Au-S), ◦	73; 56	72; 59	64; 52	68; 56

Table 4. Parameters characterizing the transition state structures for Au adatom migration along the <$\underline{1}$01> direction. Structures are displayed in Figure 4 top panel. E^f – Formation energy for the SAM phase refered to the clean Au(111) suface, gas phase $(CH_3S)_2$ and bulk Au; $z_e(Au)$ – Height of Au over the surface (111) plane; d_e(Au-S) – Interatomic distances between the Au adatom and the two nearest S atoms.

Parameter	*fcc-to-top*	*top-to-hcp*	*hcp-to-fcc*
E^f, eV	-1.48	-1.52	-2.20
z_e(Au), Å	2.491	2.410	2.461
d_e(Au-S), Å	2.456; 2.407; 3.065	2.751; 3.224; 2.348	2.330;2.342; 4.159

Table 5. Parameters characterizing the transition state structures for Au adatom migration along the <1$\underline{1}$0> direction. Structures are displayed in Figure 4 bottom panel. E^f – Formation energy for the SAM phase refered to the clean Au(111) suface, gas phase $(CH_3S)_2$ and bulk Au; $z_e(Au)$ – Height of Au over the surface (111) plane; d_e(Au-S) – Interatomic distances between the Au adatom and the two nearest S atoms.

Parameter	*fcc-to-hcp'*	*hcp'-to-fcc'*	*fcc'-to-hcp*
E^f, eV	-1.27	-2.16	-1.21
z_e(Au), Å	2.483	2.453	2.404
d_e(Au-S), Å	2.776; 2.309; 3.041	2.376; 2.466;4.173	2.814; 2.284; 3.083

Figure 1. Schematic representation of adsorption structures for a single Au adatom (grey sphere) at the different adsorption sites on the self-assembled monolayers involving two Au-S bonds. The label refers to the location of the Au adatom. For convenience the dashed line indicates the unit cell of the (√3 × √3)-R30° structure. Note, however, that a (3√3 ×3 √3)-R30°-CH_3S supercell with 9 independent MT molecules is used in the calculations.

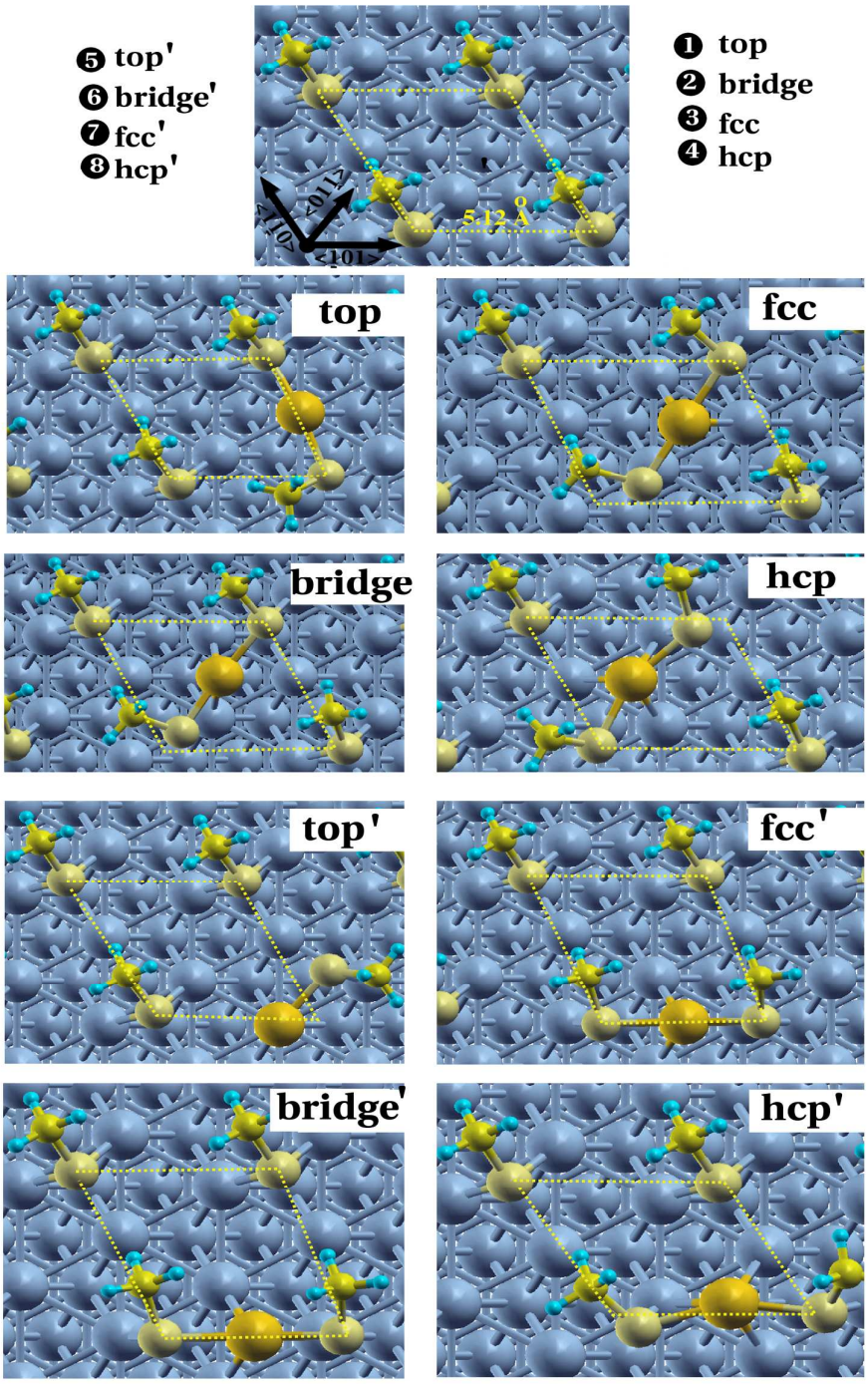

Figure 2. Schematic representations of the different CH_3S-Au-CH_3S adsorption arrangements on the Au(111) surface. The Au adatom is presented in grey to facilitate the view. The label refers to the location of the Au adatom. The adsorption configurations have been labelled as *fcc*, *hcp*, *bridge* and *top*, depending on the location of the gold adatom, which has been presented in a darker colour to facilitate the view. Note, however, that a $(3\sqrt{3} \times 3\sqrt{3})$-R30°-$CH_3S$ supercell with a single CH_3S-Au-CH_3S complex is used in the calculations

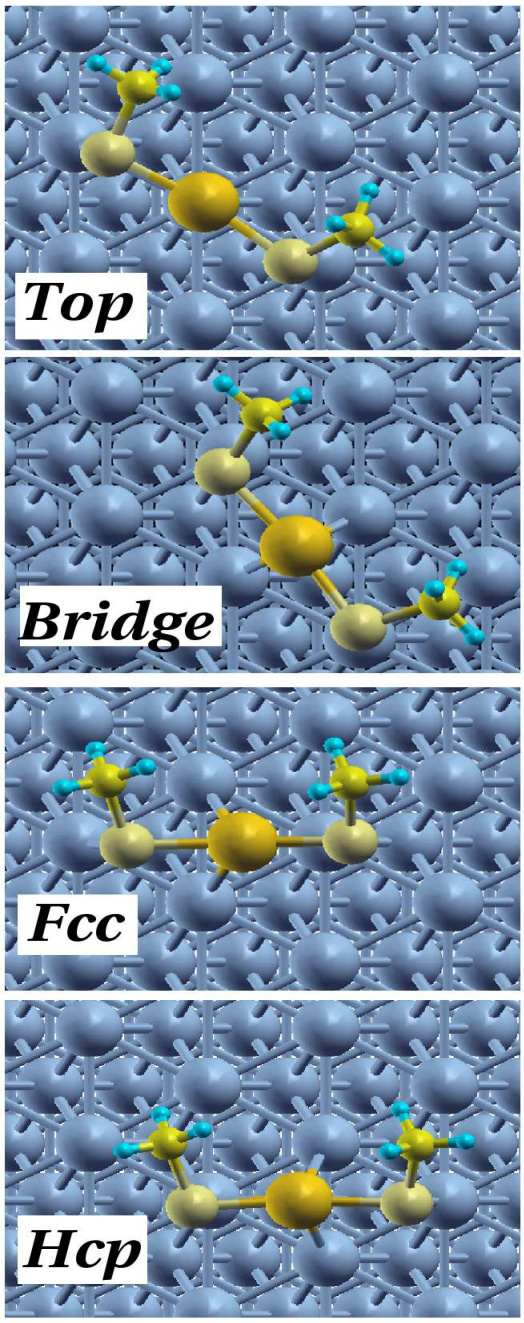

Figure 3. Density of states (DOS) plots of the most stable SCH_3-Au-SCH_3 *bridge* structure (top panel) and the SAM *fcc* structure (bottom panel). See Figure 2 and 3 for more details on the structures. DOS was further projected (PDOS) on the Au adatom (yellow solid line) and the two SCH_3 species bonded to the adatom (red line). The energy values were referred to the Fermi energy.

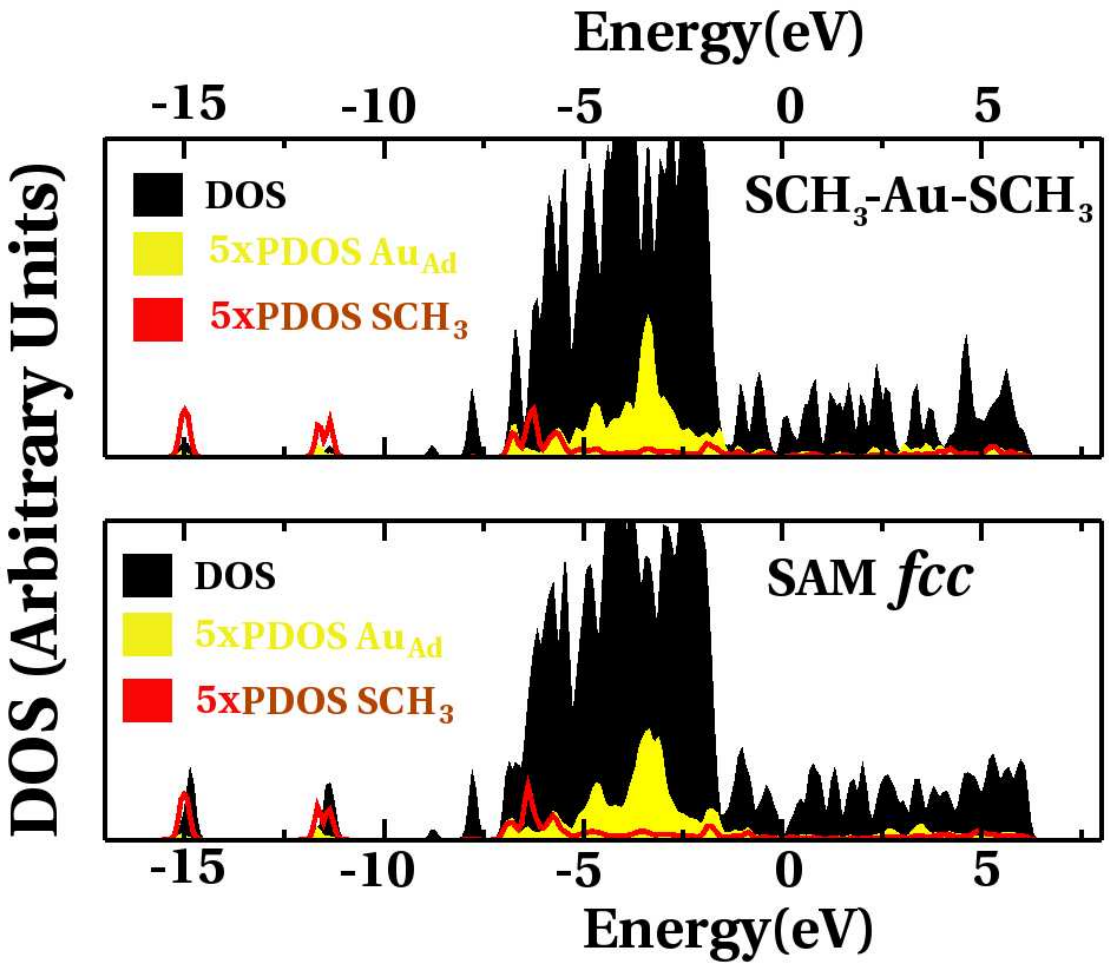

Figure 4. Central Panel: Energy diagram for the migration of a single Au adatom along the <$\underline{1}$01> and <1$\underline{1}$0> crystallographic directions. The zero energy is taken as the sum of the energies of the clean Au(111) suface, the gas phase $(CH_3S)_2$ and bulk Au. Top and Lower Panels: Schematic representation of the structures along the two different migration paths. The Au adatom is presented in a darker colour to facilitate the view.

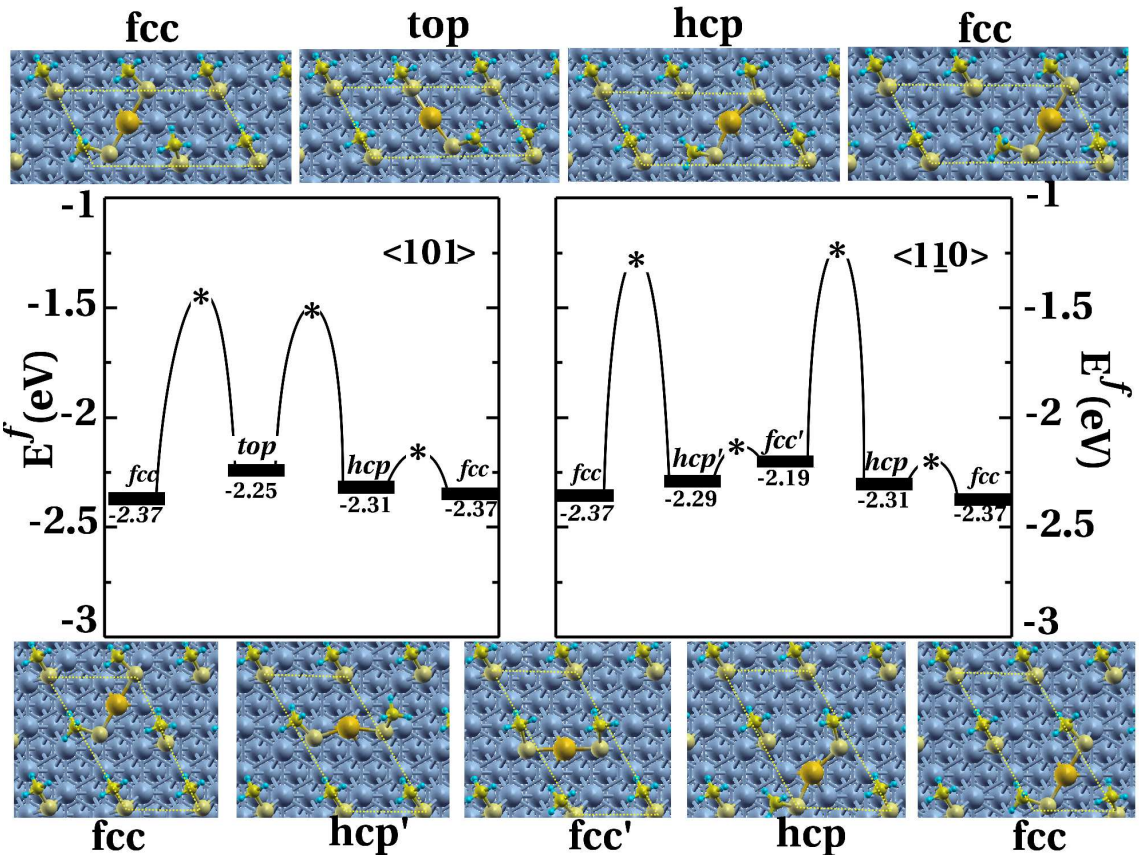

Figure 5. Schematic representation of the representative transition-state structures involved in Au migration.

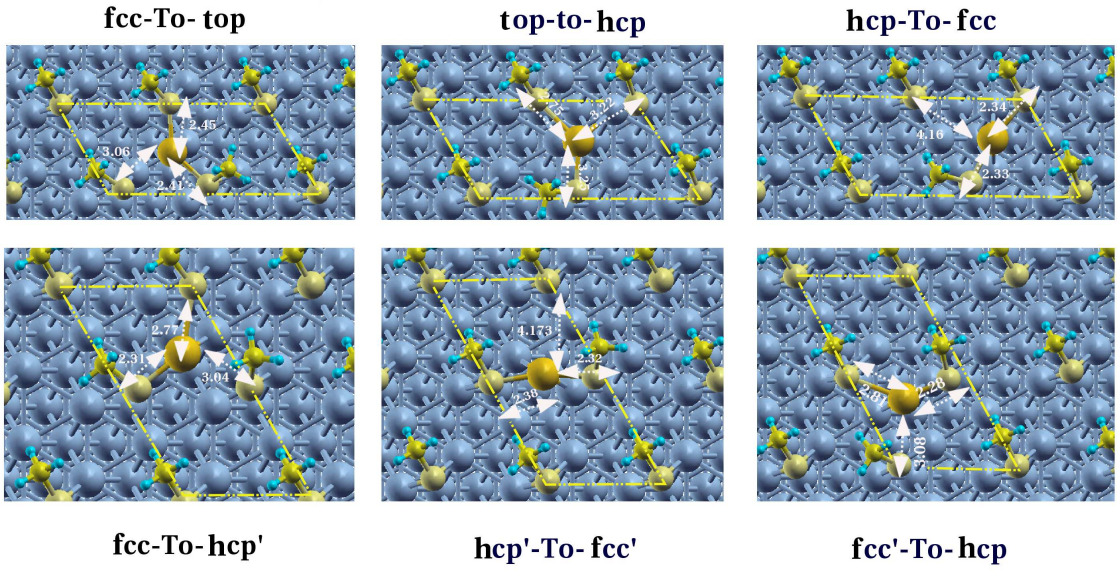

References

[1] J. C. Love, L. A. Estroff, J. K. Kriebel, R. G. Nuzzo, G. M. Whitesides, *Chem. Rev.,* 2005, **105**, 1103

[2] A. Ulman, *Chem. Rev.,* 1996, **96**, 1533

[3] O. Azzaroni, M. Cipollone, M. E. Vela, R. C. Salvarezza, *Langmuir*, 2001, **17**, 1483

[4] R. K. Smith, P. A. Lewis, P. S. Weiss, *Prog. Surf. Sci.*, 2004, **75**, 1.

[5] R. Levicky, T. M. Herne, M. J. Tarlov, S. K. Satija, *J. Am. Chem. Soc.*, 1998, **120**, 9787

[6] S. T. Marshall, M. O'Brien, B. Oetter, A. Corpuz, R. M. Richards, D. K. Schwartz, J. W. Medlin , *Nat. Mat.*, 2010, **9**, 853

[7] H. Imahori, S. Fukuzumi, *Adv. Funct. Mater.* , 2004, **14**, 525

[8] C. Vericat, M. E. Vela, G. Benitez, P. Carro, R. C. Salvarezza, *Chem. Soc. Rev.*, 2010, **39**, 1805.

[9] J. C. Azcarate, G. Corthey, E. Pensa, C. Vericat, M. H. Fonticelli, R. C. Salvarezza, P. Carro, J. Phys. *Chem. Lett.*, 2013, **4**, 3127

[10] H. Häkkinen, *Nat. Chem.*, 2012, **4**, 443

[11] G. E. Poirier, E. D. Pylant, *Science*, 1996, **272**, 1145

[12] G. E. Poirier, *Langmuir*, 1997, **13**, 2019

[13] R. Mazzarello, A. Cossaro, A. Verdini, R. Rousseau, L. Casalis, M.F. Danisman, L. Floreano, S. Scandolo, A. Morgante, G. Scoles, *Phys. Rev. Lett.*, 2007, **98**, 016102

[14] M.Yu, N. Bovet, C. J. Satterley, S. Bengió, K. R. J. Lovelock, P. K. Milligan, R. G. Jones, D. P. Woodruff, V. Dhanak, *Phys. Rev. Lett.*, 2006, **97**, 166102

[15] L. M. Molina, B. Hammer, *Chem. Phys. Lett.*, 2002, **360**, 264

[16] S.J Stranick, A.N. Parikh, D.L. Allara, P.S. Weiss, *J. Phys. Chem.*, 1994, **98**, 11136

[17] P. Maksymovych, D. S. Sorescu, J. T. Yates, Jr., *Phys. Rev. Lett.*, 2006, **97**, 146103

[18] P. Carro, D. Torres, R. Diaz, R. C. Salvarezza, F. Illas, *J. Phys. Chem. Lett.*, 2012, **3**, 2159

[19] D. Torres, P. Carro, R. C. Salvarezza, F. Illas, *Phys. Rev. Lett*, 2006, **97**, 226103

[20] G. Kresse, J. Hafner, *J. Phys. Rev. B*, 1993, **47**, 558

[21] G. Kresse, J. Furthmuller, *J. Phys. Rev. B*, 1996, **54**, 11169

[22] P. Blöchl, *Phys. Rev. B*., 1994, **50**, 17953

[23] J. Perdew, Y. Wang, *Phys. Rev. B*, 1992, **45**, 13244

[24] P. Janthon, S. M. Kozlov, F. Viñes, J. Limtrakul, F. Illas, *J. Chem. Theory and Comput.*, 2013, **9**, 1631

[25] S. González, F. Viñes, J. F. García, Y. Erazo and F. Illas, *Surf. Sci.* 2014, **625**, 64-68

[26] K. Tonigold, A. Gross, *J. Chem. Phys.* 2010, **132**, 224701

[27] P. Carro, E. Pensa, C. Vericat, R. C. Salvarezza, *J. Phys. Chem. C* 2013, **117**, 2160

[28] P. Carro, R. Salvarezza, D. Torres, F. Illas, *J. Phys. Chem. C*, 2008, **112**, 19121

[29] M. Danisman, L. Casalis, G. Bracco, G. Scoles, *J. Phys. Chem. B*, 2002, *106*, 11771

[30] C. Vericat, M. Vela, R. Salvarezza, *Phys. Chem. Chem. Phys.*, 2005, **7**, 3258; X. Torrelles, C. Vericat, M. Vela, M. Fonticelli, M. Daza Millone, R. Felici, T.-L. Lee, J. Zegenhagen, G. Munoz, J. Martin-Gago, Roberto C. Salvarezza, *J. Phys. Chem. B*, 2006, **110**, 5586

[31] G. Mills, H. Jonsson, *Phys. Rev. Lett.*, 1994, **72**, 1124

[32] G. Mills, H. Jonsson, G. K. Schenter, *Surf. Sci.*, 1995, **324**, 305

[33] G. Henkelman, B. P. Uberuaga, H. J. Jonsson, *Chem. Phys.*, 2000, **113**, 9901

[34] A. Franke, and E. Pehlke, *Phys. Rev. B*, 2009, **79**, 235441

[35] G.S. Longo, S. Kr. Bhattachrya, S. Scandolo, *J. Phys. Chem. C*, 2012, **116**, 14883